

Trigger and Aperture of the Surface Detector Array of the Pierre Auger Observatory

The Pierre Auger Collaboration

J. Abraham⁸, P. Abreu⁷¹, M. Aglietta⁵⁴, C. Aguirre¹², E.J. Ahn⁸⁷,
D. Allard³¹, I. Allekotte¹, J. Allen⁹⁰, J. Alvarez-Muñiz⁷⁸, M. Ambrosio⁴⁸,
L. Anchordoqui¹⁰⁴, S. Andringa⁷¹, A. Anzalone⁵³, C. Aramo⁴⁸,
E. Arganda⁷⁵, S. Argirò⁵¹, K. Arisaka⁹⁵, F. Arneodo⁵⁵, F. Arqueros⁷⁵,
T. Asch³⁸, H. Asorey¹, P. Assis⁷¹, J. Aublin³³, M. Ave⁹⁶, G. Avila¹⁰,
T. Bäcker⁴², D. Badagnani⁶, K.B. Barber¹¹, A.F. Barbosa¹⁴,
S.L.C. Barroso²⁰, B. Baughman⁹², P. Bauleo⁸⁵, J.J. Beatty⁹², T. Beau³¹,
B.R. Becker¹⁰¹, K.H. Becker³⁶, A. Bellétoile³⁴, J.A. Bellido^{11, 93},
S. BenZvi¹⁰³, C. Berat³⁴, P. Bernardini⁴⁷, X. Bertou¹, P.L. Biermann³⁹,
P. Billoir³³, O. Blanch-Bigas³³, F. Blanco⁷⁵, C. Bleve⁴⁷, H. Blümer^{41, 37},
M. Boháčová^{96, 27}, D. Boncioli⁴⁹, C. Bonifazi³³, R. Bonino⁵⁴, N. Borodai⁶⁹,
J. Brack⁸⁵, P. Brogueira⁷¹, W.C. Brown⁸⁶, R. Bruijn⁸¹, P. Buchholz⁴²,
A. Bueno⁷⁷, R.E. Burton⁸³, N.G. Busca³¹, K.S. Caballero-Mora⁴¹,
L. Caramete³⁹, R. Caruso⁵⁰, W. Carvalho¹⁷, A. Castellina⁵⁴, O. Catalano⁵³,
L. Cazon⁹⁶, R. Cester⁵¹, J. Chauvin³⁴, A. Chiavassa⁵⁴, J.A. Chinellato¹⁸,
A. Chou^{87, 90}, J. Chudoba²⁷, J. Chye^{89 d}, R.W. Clay¹¹, E. Colombo²,
R. Conceição⁷¹, B. Connolly¹⁰², F. Contreras⁹, J. Coppens^{65, 67},
A. Cordier³², U. Cotti⁶³, S. Coutu⁹³, C.E. Covault⁸³, A. Creusot⁷³,
A. Criss⁹³, J. Cronin⁹⁶, A. Curutiu³⁹, S. Dagoret-Campagne³², R. Dallier³⁵,
K. Daumiller³⁷, B.R. Dawson¹¹, R.M. de Almeida¹⁸, M. De Domenico⁵⁰,
C. De Donato⁴⁶, S.J. de Jong⁶⁵, G. De La Vega⁸, W.J.M. de Mello Junior¹⁸,
J.R.T. de Mello Neto²³, I. De Mitri⁴⁷, V. de Souza¹⁶, K.D. de Vries⁶⁶,
G. Decerprit³¹, L. del Peral⁷⁶, O. Deligny³⁰, A. Della Selva⁴⁸, C. Delle
Fratte⁴⁹, H. Dembinski⁴⁰, C. Di Giulio⁴⁹, J.C. Diaz⁸⁹, P.N. Diep¹⁰⁵,
C. Dobrigkeit¹⁸, J.C. D'Olivo⁶⁴, P.N. Dong¹⁰⁵, A. Dorofeev^{85, 88}, J.C. dos
Anjos¹⁴, M.T. Dova⁶, D. D'Urso⁴⁸, I. Dutan³⁹, M.A. DuVernois⁹⁸,
R. Engel³⁷, M. Erdmann⁴⁰, C.O. Escobar¹⁸, A. Etchegoyen², P. Facal San
Luis^{96, 78}, H. Falcke^{65, 68}, G. Farrar⁹⁰, A.C. Fauth¹⁸, N. Fazzini⁸⁷,
F. Ferrer⁸³, A. Ferrero², B. Fick⁸⁹, A. Filevich², A. Filipčić^{72, 73}, I. Fleck⁴²,
S. Fliescher⁴⁰, C.E. Fracchiolla⁸⁵, E.D. Fraenkel⁶⁶, W. Fulgione⁵⁴,

*Corresponding author. Email address: giorgio.matthiae@roma2.infn.it

R.F. Gamarra², S. Gambetta⁴⁴, B. García⁸, D. García Gámez⁷⁷,
 D. Garcia-Pinto⁷⁵, X. Garrido^{37, 32}, G. Gelmini⁹⁵, H. Gemmeke³⁸,
 P.L. Ghia^{30, 54}, U. Giaccari⁴⁷, M. Giller⁷⁰, H. Glass⁸⁷, L.M. Goggin¹⁰⁴,
 M.S. Gold¹⁰¹, G. Golup¹, F. Gomez Albarracin⁶, M. Gómez Berisso¹,
 P. Gonçalves⁷¹, M. Gonçalves do Amaral²⁴, D. Gonzalez⁴¹,
 J.G. Gonzalez^{77, 88}, D. Góra^{41, 69}, A. Gorgi⁵⁴, P. Gouffon¹⁷, S.R. Gozzini⁸¹,
 E. Grashorn⁹², S. Grebe⁶⁵, M. Grigat⁴⁰, A.F. Grillo⁵⁵, Y. Guardincerri⁴,
 F. Guarino⁴⁸, G.P. Guedes¹⁹, J. Gutiérrez⁷⁶, J.D. Hague¹⁰¹, V. Halenka²⁸,
 P. Hansen⁶, D. Harari¹, S. Harmsma^{66, 67}, J.L. Harton⁸⁵, A. Haungs³⁷,
 M.D. Healy⁹⁵, T. Hebbeker⁴⁰, G. Hebrero⁷⁶, D. Heck³⁷, C. Hojvat⁸⁷,
 V.C. Holmes¹¹, P. Homola⁶⁹, J.R. Hörandel⁶⁵, A. Horneffer⁶⁵,
 M. Hrabovský^{28, 27}, T. Huege³⁷, M. Hussain⁷³, M. Iarlori⁴⁵, A. Insolia⁵⁰,
 F. Ionita⁹⁶, A. Italiano⁵⁰, S. Jiraskova⁶⁵, M. Kaducak⁸⁷, K.H. Kampert³⁶,
 T. Karova²⁷, P. Kasper⁸⁷, B. Kégl³², B. Keilhauer³⁷, E. Kemp¹⁸,
 R.M. Kieckhafer⁸⁹, H.O. Klages³⁷, M. Kleifges³⁸, J. Kleinfeller³⁷,
 R. Knapik⁸⁵, J. Knapp⁸¹, D.-H. Koang³⁴, A. Krieger², O. Krömer³⁸,
 D. Kruppke-Hansen³⁶, F. Kuehn⁸⁷, D. Kuempel³⁶, K. Kulbartz⁴³,
 N. Kunka³⁸, A. Kusenko⁹⁵, G. La Rosa⁵³, C. Lachaud³¹, B.L. Lago²³,
 P. Lautridou³⁵, M.S.A.B. Leão²², D. Lebrun³⁴, P. Lebrun⁸⁷, J. Lee⁹⁵,
 M.A. Leigui de Oliveira²², A. Lemiere³⁰, A. Letessier-Selvon³³,
 M. Leuthold⁴⁰, I. Lhenry-Yvon³⁰, R. López⁵⁹, A. Lopez Agüera⁷⁸,
 K. Louedec³², J. Lozano Bahilo⁷⁷, A. Lucero⁵⁴, H. Lyberis³⁰,
 M.C. Maccarone⁵³, C. Macolino⁴⁵, S. Maldera⁵⁴, D. Mandat²⁷,
 P. Mantsch⁸⁷, A.G. Mariazzi⁶, I.C. Maris⁴¹, H.R. Marquez Falcon⁶³,
 D. Martello⁴⁷, O. Martínez Bravo⁵⁹, H.J. Mathes³⁷, J. Matthews^{88, 94},
 J.A.J. Matthews¹⁰¹, G. Matthiae^{49*}, D. Maurizio⁵¹, P.O. Mazur⁸⁷,
 M. McEwen⁷⁶, R.R. McNeil⁸⁸, G. Medina-Tanco⁶⁴, M. Melissas⁴¹,
 D. Melo⁵¹, E. Menichetti⁵¹, A. Menshikov³⁸, R. Meyhandan¹⁴,
 M.I. Micheletti², G. Miele⁴⁸, W. Miller¹⁰¹, L. Miramonti⁴⁶, S. Mollerach¹,
 M. Monasor⁷⁵, D. Monnier Ragainne³², F. Montanet³⁴, B. Morales⁶⁴,
 C. Morello⁵⁴, J.C. Moreno⁶, C. Morris⁹², M. Mostafá⁸⁵, C.A. Moura⁴⁸,
 S. Mueller³⁷, M.A. Muller¹⁸, R. Mussa⁵¹, G. Navarra⁵⁴, J.L. Navarro⁷⁷,
 S. Navas⁷⁷, P. Necasal²⁷, L. Nellen⁶⁴, C. Newman-Holmes⁸⁷, D. Newton⁸¹,
 P.T. Nhung¹⁰⁵, N. Nierstenhoefer³⁶, D. Nitz⁸⁹, D. Nosek²⁶, L. Nožka²⁷,
 M. Nyklicek²⁷, J. Oehlschläger³⁷, A. Olinto⁹⁶, P. Oliva³⁶,
 V.M. Olmos-Gilbaja⁷⁸, M. Ortiz⁷⁵, N. Pacheco⁷⁶, D. Pakk Selmi-Dei¹⁸,
 M. Palatka²⁷, J. Pallotta³, G. Parente⁷⁸, E. Parizot³¹, S. Parlati⁵⁵,
 S. Pastor⁷⁴, M. Patel⁸¹, T. Paul⁹¹, V. Pavlidou^{96 c}, K. Payet³⁴, M. Pech²⁷,

J. Pękala⁶⁹, I.M. Pepe²¹, L. Perrone⁵², R. Pesce⁴⁴, E. Petermann¹⁰⁰,
 S. Petrerá⁴⁵, P. Petrinca⁴⁹, A. Petrolini⁴⁴, Y. Petrov⁸⁵, J. Petrovic⁶⁷,
 C. Pfendner¹⁰³, R. Piegáia⁴, T. Pierog³⁷, M. Pimenta⁷¹, T. Pinto⁷⁴,
 V. Pirronello⁵⁰, O. Pisanti⁴⁸, M. Platino², J. Pochon¹, V.H. Ponce¹,
 M. Pontz⁴², P. Privitera⁹⁶, M. Prouza²⁷, E.J. Quel³, J. Rautenberg³⁶,
 O. Ravel³⁵, D. Ravignani², A. Redondo⁷⁶, B. Revenu³⁵, F.A.S. Rezende¹⁴,
 J. Ridky²⁷, S. Riggi⁵⁰, M. Risse³⁶, C. Rivière³⁴, V. Rizi⁴⁵, C. Robledo⁵⁹,
 G. Rodriguez⁴⁹, J. Rodriguez Martino⁵⁰, J. Rodriguez Rojo⁹,
 I. Rodriguez-Cabo⁷⁸, M.D. Rodríguez-Frías⁷⁶, G. Ros^{75, 76}, J. Rosado⁷⁵,
 T. Rossler²⁸, M. Roth³⁷, B. Rouillé-d'Orfeuill³¹, E. Roulet¹, A.C. Rovero⁷,
 F. Salamida⁴⁵, H. Salazar^{59 b}, G. Salina⁴⁹, F. Sánchez⁶⁴, M. Santander⁹,
 C.E. Santo⁷¹, E.M. Santos²³, F. Sarazin⁸⁴, S. Sarkar⁷⁹, R. Sato⁹, N. Scharf⁴⁰,
 V. Scherini³⁶, H. Schieler³⁷, P. Schiffer⁴⁰, A. Schmidt³⁸, F. Schmidt⁹⁶,
 T. Schmidt⁴¹, O. Scholten⁶⁶, H. Schoorlemmer⁶⁵, J. Schovancova²⁷,
 P. Schovánek²⁷, F. Schroeder³⁷, S. Schulte⁴⁰, F. Schüssler³⁷, D. Schuster⁸⁴,
 S.J. Scitutto⁶, M. Scuderi⁵⁰, A. Segreto⁵³, D. Semikoz³¹, M. Settimo⁴⁷,
 R.C. Shellard^{14, 15}, I. Sidelnik², B.B. Siffert²³, G. Sigl⁴³, A. Śmiałkowski⁷⁰,
 R. Šmída²⁷, B.E. Smith⁸¹, G.R. Snow¹⁰⁰, P. Sommers⁹³, J. Sorokin¹¹,
 H. Spinka^{82, 87}, R. Squartini⁹, E. Strazzeri³², A. Stutz³⁴, F. Suarez²,
 T. Suomijärvi³⁰, A.D. Supanitsky⁶⁴, M.S. Sutherland⁹², J. Swain⁹¹,
 Z. Szadkowski⁷⁰, A. Tamashiro⁷, A. Tamburro⁴¹, T. Tarutina⁶, O. Taşcău³⁶,
 R. Tcaciuc⁴², D. Tcherniakhovskii³⁸, D. Tegolo⁵⁸, N.T. Thao¹⁰⁵,
 D. Thomas⁸⁵, R. Ticona¹³, J. Tiffenberg⁴, C. Timmermans^{67, 65},
 W. Tkaczyk⁷⁰, C.J. Todero Peixoto²², B. Tomé⁷¹, A. Tonachini⁵¹,
 I. Torres⁵⁹, P. Travnicek²⁷, D.B. Tridapalli¹⁷, G. Tristram³¹, E. Trovato⁵⁰,
 M. Tueros⁶, R. Ulrich³⁷, M. Unger³⁷, M. Urban³², J.F. Valdés Galicia⁶⁴,
 I. Valiño³⁷, L. Valore⁴⁸, A.M. van den Berg⁶⁶, J.R. Vázquez⁷⁵,
 R.A. Vázquez⁷⁸, D. Veberič^{73, 72}, A. Velarde¹³, T. Venters⁹⁶, V. Verzi⁴⁹,
 M. Videla⁸, L. Villaseñor⁶³, S. Vorobiov⁷³, L. Voyvodic^{87 †}, H. Wahlberg⁶,
 P. Wahrlich¹¹, O. Wainberg², D. Warner⁸⁵, A.A. Watson⁸¹, S. Westerhoff¹⁰³,
 B.J. Whelan¹¹, G. Wiczorek⁷⁰, L. Wiencke⁸⁴, B. Wilczyńska⁶⁹,
 H. Wilczyński⁶⁹, C. Wileman⁸¹, M.G. Winnick¹¹, H. Wu³², B. Wundheiler²,
 T. Yamamoto^{96 a}, P. Younk⁸⁵, G. Yuan⁸⁸, A. Yushkov⁴⁸, E. Zas⁷⁸,
 D. Zavrtnik^{73, 72}, M. Zavrtnik^{72, 73}, I. Zaw⁹⁰, A. Zepeda^{60 b},
 M. Ziolkowski⁴²

¹ *Centro Atómico Bariloche and Instituto Balseiro (CNEA- UNCuyo-CONICET), San Carlos de Bariloche, Argentina*

² *Centro Atómico Constituyentes (Comisión Nacional de Energía*

- Atómica/CONICET/UTN-FRBA), Buenos Aires, Argentina*
- ³ *Centro de Investigaciones en Láseres y Aplicaciones, CITEFA and CONICET, Argentina*
- ⁴ *Departamento de Física, FCEyN, Universidad de Buenos Aires y CONICET, Argentina*
- ⁶ *IFLP, Universidad Nacional de La Plata and CONICET, La Plata, Argentina*
- ⁷ *Instituto de Astronomía y Física del Espacio (CONICET), Buenos Aires, Argentina*
- ⁸ *National Technological University, Faculty Mendoza (CONICET/CNEA), Mendoza, Argentina*
- ⁹ *Pierre Auger Southern Observatory, Malargüe, Argentina*
- ¹⁰ *Pierre Auger Southern Observatory and Comisión Nacional de Energía Atómica, Malargüe, Argentina*
- ¹¹ *University of Adelaide, Adelaide, S.A., Australia*
- ¹² *Universidad Católica de Bolivia, La Paz, Bolivia*
- ¹³ *Universidad Mayor de San Andrés, Bolivia*
- ¹⁴ *Centro Brasileiro de Pesquisas Físicas, Rio de Janeiro, RJ, Brazil*
- ¹⁵ *Pontifícia Universidade Católica, Rio de Janeiro, RJ, Brazil*
- ¹⁶ *Universidade de São Paulo, Instituto de Física, São Carlos, SP, Brazil*
- ¹⁷ *Universidade de São Paulo, Instituto de Física, São Paulo, SP, Brazil*
- ¹⁸ *Universidade Estadual de Campinas, IFGW, Campinas, SP, Brazil*
- ¹⁹ *Universidade Estadual de Feira de Santana, Brazil*
- ²⁰ *Universidade Estadual do Sudoeste da Bahia, Vitória da Conquista, BA, Brazil*
- ²¹ *Universidade Federal da Bahia, Salvador, BA, Brazil*
- ²² *Universidade Federal do ABC, Santo André, SP, Brazil*
- ²³ *Universidade Federal do Rio de Janeiro, Instituto de Física, Rio de Janeiro, RJ, Brazil*
- ²⁴ *Universidade Federal Fluminense, Instituto de Física, Niterói, RJ, Brazil*
- ²⁶ *Charles University, Faculty of Mathematics and Physics, Institute of Particle and Nuclear Physics, Prague, Czech Republic*
- ²⁷ *Institute of Physics of the Academy of Sciences of the Czech Republic, Prague, Czech Republic*
- ²⁸ *Palacký University, Olomouc, Czech Republic*
- ³⁰ *Institut de Physique Nucléaire d'Orsay (IPNO), Université Paris 11, CNRS-IN2P3, Orsay, France*
- ³¹ *Laboratoire AstroParticule et Cosmologie (APC), Université Paris 7, CNRS-IN2P3, Paris, France*
- ³² *Laboratoire de l'Accélérateur Linéaire (LAL), Université Paris 11, CNRS-IN2P3, Orsay, France*
- ³³ *Laboratoire de Physique Nucléaire et de Hautes Energies (LPNHE), Universités Paris 6 et Paris 7, Paris Cedex 05, France*
- ³⁴ *Laboratoire de Physique Subatomique et de Cosmologie (LPSC), Université Joseph Fourier, INPG, CNRS-IN2P3, Grenoble, France*
- ³⁵ *SUBATECH, Nantes, France*
- ³⁶ *Bergische Universität Wuppertal, Wuppertal, Germany*
- ³⁷ *Forschungszentrum Karlsruhe, Institut für Kernphysik, Karlsruhe, Germany*
- ³⁸ *Forschungszentrum Karlsruhe, Institut für Prozessdatenverarbeitung und Elektronik, Karlsruhe, Germany*

- ³⁹ *Max-Planck-Institut für Radioastronomie, Bonn, Germany*
- ⁴⁰ *RWTH Aachen University, III. Physikalisches Institut A, Aachen, Germany*
- ⁴¹ *Universität Karlsruhe (TH), Institut für Experimentelle Kernphysik (IEKP), Karlsruhe, Germany*
- ⁴² *Universität Siegen, Siegen, Germany*
- ⁴³ *Universität Hamburg, Hamburg, Germany*
- ⁴⁴ *Dipartimento di Fisica dell'Università and INFN, Genova, Italy*
- ⁴⁵ *Università dell'Aquila and INFN, L'Aquila, Italy*
- ⁴⁶ *Università di Milano and Sezione INFN, Milan, Italy*
- ⁴⁷ *Dipartimento di Fisica dell'Università del Salento and Sezione INFN, Lecce, Italy*
- ⁴⁸ *Università di Napoli "Federico II" and Sezione INFN, Napoli, Italy*
- ⁴⁹ *Università di Roma II "Tor Vergata" and Sezione INFN, Roma, Italy*
- ⁵⁰ *Università di Catania and Sezione INFN, Catania, Italy*
- ⁵¹ *Università di Torino and Sezione INFN, Torino, Italy*
- ⁵² *Dipartimento di Ingegneria dell'Innovazione dell'Università del Salento and Sezione INFN, Lecce, Italy*
- ⁵³ *Istituto di Astrofisica Spaziale e Fisica Cosmica di Palermo (INAF), Palermo, Italy*
- ⁵⁴ *Istituto di Fisica dello Spazio Interplanetario (INAF), Università di Torino and Sezione INFN, Torino, Italy*
- ⁵⁵ *INFN, Laboratori Nazionali del Gran Sasso, Assergi (L'Aquila), Italy*
- ⁵⁸ *Università di Palermo and Sezione INFN, Catania, Italy*
- ⁵⁹ *Benemérita Universidad Autónoma de Puebla, Puebla, Mexico*
- ⁶⁰ *Centro de Investigación y de Estudios Avanzados del IPN (CINVESTAV), México, D.F., Mexico*
- ⁶¹ *Instituto Nacional de Astrofisica, Optica y Electronica, Tonantzintla, Puebla, Mexico*
- ⁶³ *Universidad Michoacana de San Nicolas de Hidalgo, Morelia, Michoacan, Mexico*
- ⁶⁴ *Universidad Nacional Autonoma de Mexico, Mexico, D.F., Mexico*
- ⁶⁵ *IMAPP, Radboud University, Nijmegen, Netherlands*
- ⁶⁶ *Kernfysisch Versneller Instituut, University of Groningen, Groningen, Netherlands*
- ⁶⁷ *NIKHEF, Amsterdam, Netherlands*
- ⁶⁸ *ASTRON, Dwingeloo, Netherlands*
- ⁶⁹ *Institute of Nuclear Physics PAN, Krakow, Poland*
- ⁷⁰ *University of Łódź, Łódź, Poland*
- ⁷¹ *LIP and Instituto Superior Técnico, Lisboa, Portugal*
- ⁷² *J. Stefan Institute, Ljubljana, Slovenia*
- ⁷³ *Laboratory for Astroparticle Physics, University of Nova Gorica, Slovenia*
- ⁷⁴ *Instituto de Física Corpuscular, CSIC-Universitat de València, Valencia, Spain*
- ⁷⁵ *Universidad Complutense de Madrid, Madrid, Spain*
- ⁷⁶ *Universidad de Alcalá, Alcalá de Henares (Madrid), Spain*
- ⁷⁷ *Universidad de Granada & C.A.F.P.E., Granada, Spain*
- ⁷⁸ *Universidad de Santiago de Compostela, Spain*
- ⁷⁹ *Rudolf Peierls Centre for Theoretical Physics, University of Oxford, Oxford, United Kingdom*
- ⁸¹ *School of Physics and Astronomy, University of Leeds, United Kingdom*
- ⁸² *Argonne National Laboratory, Argonne, IL, USA*

- ⁸³ *Case Western Reserve University, Cleveland, OH, USA*
⁸⁴ *Colorado School of Mines, Golden, CO, USA*
⁸⁵ *Colorado State University, Fort Collins, CO, USA*
⁸⁶ *Colorado State University, Pueblo, CO, USA*
⁸⁷ *Fermilab, Batavia, IL, USA*
⁸⁸ *Louisiana State University, Baton Rouge, LA, USA*
⁸⁹ *Michigan Technological University, Houghton, MI, USA*
⁹⁰ *New York University, New York, NY, USA*
⁹¹ *Northeastern University, Boston, MA, USA*
⁹² *Ohio State University, Columbus, OH, USA*
⁹³ *Pennsylvania State University, University Park, PA, USA*
⁹⁴ *Southern University, Baton Rouge, LA, USA*
⁹⁵ *University of California, Los Angeles, CA, USA*
⁹⁶ *University of Chicago, Enrico Fermi Institute, Chicago, IL, USA*
⁹⁸ *University of Hawaii, Honolulu, HI, USA*
¹⁰⁰ *University of Nebraska, Lincoln, NE, USA*
¹⁰¹ *University of New Mexico, Albuquerque, NM, USA*
¹⁰² *University of Pennsylvania, Philadelphia, PA, USA*
¹⁰³ *University of Wisconsin, Madison, WI, USA*
¹⁰⁴ *University of Wisconsin, Milwaukee, WI, USA*
¹⁰⁵ *Institute for Nuclear Science and Technology (INST), Hanoi, Vietnam*
‡) *Deceased*
(a) *at Konan University, Kobe, Japan*
(b) *On leave of absence at the Instituto Nacional de Astrofisica, Optica y Electronica*
(c) *at Caltech, Pasadena, USA*
(d) *at Hawaii Pacific University*

Abstract

The surface detector array of the Pierre Auger Observatory consists of 1600 water-Cherenkov detectors, for the study of extensive air showers (EAS) generated by ultra-high-energy cosmic rays. We describe the trigger hierarchy, from the identification of candidate showers at the level of a single detector, amongst a large background (mainly random single cosmic ray muons), up to the selection of real events and the rejection of random coincidences. Such trigger makes the surface detector array fully efficient for the detection of EAS with energy above 3×10^{18} eV, for all zenith angles between 0° and 60° , independently of the position of the impact point and of the mass of the primary particle. In these range of energies and angles, the exposure of the surface array can be determined purely on the basis of the geometrical

acceptance.

Key words: Ultra high energy cosmic rays, Auger Observatory, Extensive air showers, Trigger, Exposure

PACS: 95.85.Ry, 96.40.Pq

1. Introduction

The main objective of the Pierre Auger Collaboration is to measure the flux, arrival direction distribution and mass composition of cosmic rays from $\approx 10^{18}$ eV up to the highest energies. Due to the very low fluxes at these energies, cosmic rays have to be measured through the *extensive air showers* (EAS) they produce in the atmosphere.

The Pierre Auger Observatory, located near Malargüe, Argentina, at 1400 m asl, detects EAS in two independent and complementary ways. It includes a *surface detector array* (SD), consisting of 1600 water-Cherenkov detectors [1] on a triangular grid of 1.5 km spacing covering an area of approximately 3000 km², which detects the secondary particles at ground level and thus samples their lateral density distribution. The surface detector array is overlooked by a *fluorescence detector* (FD) consisting of 24 telescopes at four sites, which measure the fluorescence light emitted along the path of the air-showers and thus traces their longitudinal development [2]. Showers detected by both detectors are called *hybrid events* and they are characterised more accurately with respect to direction and energy than using either technique alone. However, the livetime of the FD is limited to $\approx 13\%$, as it only operates on clear, moonless nights [2]. The bulk of data is provided by the SD with its nearly 100% livetime. The study of the trigger and the determination of the aperture of the SD is thus essential for the physics aims of the Pierre Auger Observatory.

The SD data acquisition (DAQ) trigger must fulfill both physical and technical requirements. The main limitation to the rate of recordable events comes from the wireless communication system which connects the surface detectors to the central campus. The latter must serve continuously 1600 stations spread over 3000 km², each using an emitter consuming less than 1 W power to transmit to collectors as far as 40 km away. The maximum sustainable rate of events per detector is less than one per hour, to be compared to the 3 kHz counting rate per station, due to the atmospheric muon flux. The trigger thus must reduce the single station rate, without induc-

32 ing loss of physics events. It must also allow data acquisition down to the
33 lowest possible energy. To deal with all these requirements, the design of
34 the DAQ SD trigger (described in section 3) has been realised in a hierar-
35 chical form, where at each level the single station rate becomes less and less,
36 by means of discrimination against background stricter and stricter. At the
37 same time, the DAQ trigger is designed to allow the storage of the largest
38 possible number of EAS candidates .

39 The ultimate discrimination of EAS from chance events due to combina-
40 torial coincidences among the surface detectors is performed off-line through
41 a selection of physics events, and of detectors participating in each of them.
42 The event selection procedure is hierarchical too, it is described in section 4.

43 In section 5.1, we show that the trigger and event selection hierarchy
44 makes the array fully efficient for the detection of showers above 3×10^{18} eV.
45 We restrict ourselves to this energy range for the calculation of the exposure
46 (described in section 5.2), which is simply proportional to the observation
47 time and to the geometrical size of the SD array. Under these conditions the
48 calculation of the exposure is very robust and almost devoid of systematic
49 uncertainties. Therefore it is straightforward to calculate the cosmic ray flux
50 as the ratio of the number of collected events to the effective, as it was done
51 in the measurement of the cosmic ray spectrum by the surface detector of
52 Auger [3].

53 **2. The surface detector of the Pierre Auger Observatory**

54 Each water Cherenkov detector of the surface array has a 10 m^2 water
55 surface area and 1.2 m water depth, with three 9" photomultiplier tubes
56 (PMTs) looking through optical coupling material into the water volume,
57 which is contained in a Tyvek[®] reflective liner [1, 4]. Each detector operates
58 autonomously, with its own electronics and communications systems powered
59 by solar energy. Each PMT provides two signals, which are digitised by 40
60 MHz 10-bit Flash Analog to Digital Converters (FADCs). One signal is
61 directly taken from the anode of the PMT, and the other signal is provided
62 by the last dynode, amplified and inverted within the PMT base electronics to
63 a total signal nominally 32 times the anode signal. The two signals are used
64 to provide sufficient dynamic range to cover with good precision both the
65 signals produced in the detectors near the shower core ($\sim 1000 \text{ particles}/\mu\text{s}$)
66 and those produced far from the shower core ($\sim 1 \text{ particle}/\mu\text{s}$). Each FADC
67 bin corresponds to 25 ns [4].

68 The signals from the three PMTs are sent to a central data acquisition system
69 (CDAS) once a candidate shower event triggers the surface detector array (see
70 section 3.2). The total bandwidth available for data transmission from the
71 detectors to the CDAS is 1200 bits per second, which precludes the possibility
72 of any remote calibration. For this reason, the calibration of each detector
73 is performed locally and automatically. It relies on the measurement of the
74 average charge collected by a PMT from the Cherenkov light produced by a
75 vertical and central through-going muon, Q_{VEM} [5]. The water-Cherenkov
76 detector in its normal configuration has no way to select only vertical muons.
77 However, the distribution of the light of atmospheric muons produces a peak
78 in the charge distribution, Q_{VEM}^{peak} (or VEM in short), as well as a peak in
79 that of the pulse height, I_{VEM}^{peak} , both of them being proportional to those
80 produced by a vertical through-going muon. The calibration parameters are
81 determined with 2% accuracy every 60 s and returned to the CDAS with
82 each event. Due to the limited bandwidth, the first level triggers are also
83 performed locally. These triggers (section 3.1) are set in electronic units
84 (channels): the reference unit is I_{VEM}^{peak} .

85 With respect to shower reconstruction, the signals recorded by the detec-
86 tors - evaluated by integrating the FADC bins of the traces - are converted
87 to units of Q_{VEM} . These are fitted with a measured Lateral Distribution
88 Function (LDF) [11], that describes $S(r)$, the signals as a function of dis-
89 tance r from the shower core, to find the signal at 1000 m, $S(1000)$ [6]. The
90 variation of $S(1000)$ with zenith angle θ arising from the evolution of the
91 shower, is quantified by applying the constant integral intensity cut method
92 [7], justified by the approximately isotropic flux of primary cosmic rays. An
93 energy estimator for each event, independent of θ , is S_{38} , the $S(1000)$ that
94 EAS would have produced had they arrived at the median zenith angle, 38° .
95 The energy corresponding to each S_{38} is then obtained through a calibration
96 with the fluorescence detector based on a subset of high-quality hybrid events
97 [3].

98 3. The DAQ trigger system of the surface detector array

99 The trigger for the surface detector array is hierarchical. Two levels of
100 trigger (called T1 and T2) are formed at each detector. T2 triggers are com-
101 bined with those from other detectors and examined for spatial and temporal
102 correlations, leading to an array trigger (T3). The T3 trigger initiates data

103 acquisition and storage. The logic of this trigger system is summarised in
 104 figure 1.

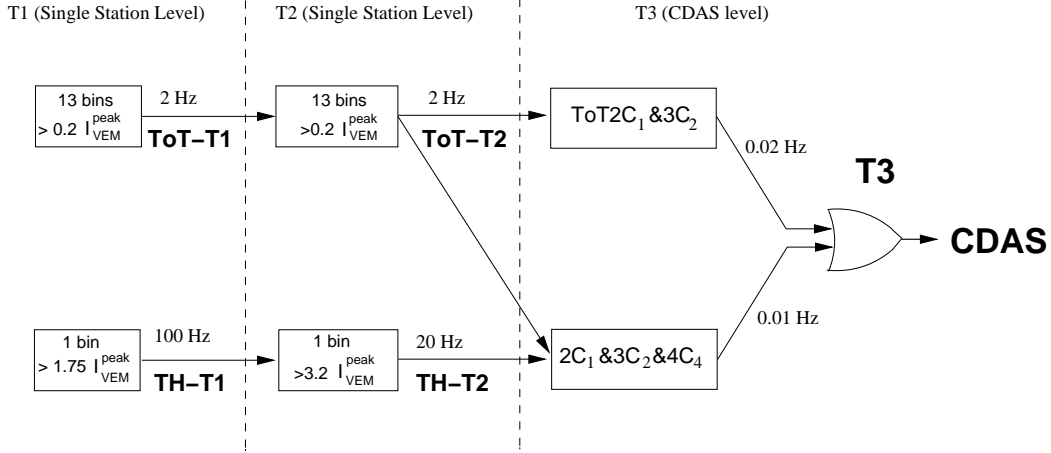


Figure 1: Schematics of the hierarchy of the trigger system of the Auger surface detector.

105 3.1. Single detector triggers

106 The **T1** triggers data acquisition in each water Cherenkov detector: data
 107 are stored on the local disk for 10 s waiting for a possible T3. Two independ-
 108 ent trigger modes are implemented as T1, having been conceived to detect,
 109 in a complementary way, the electromagnetic and muonic components of an
 110 air-shower. The first T1 mode is a simple threshold trigger (TH) which re-
 111 quires the coincidence of the three PMTs each above $1.75 I_{VEM}^{peak}$ ¹. This trigger
 112 is used to select large signals that are not necessarily spread in time. It is par-
 113 ticularly effective for the detection of very inclined showers that have crossed
 114 a large amount of atmosphere and are consequently dominantly muonic. The
 115 TH-T1 trigger is used to reduce the rate due to atmospheric muons from ≈ 3
 116 kHz to ≈ 100 Hz. The second T1 mode makes use of the fact that, for other
 117 than very inclined showers or signals from more vertical showers very close
 118 to the shower axis, the arrival of particles and photons at the detector is
 119 dispersed in time [8, 9]. For example, at 1000 m from the axis of a vertical
 120 shower, the time for the signal from a water-Cherenkov detector to rise from
 121 10 to 50% is about 300 ns. The second mode is designated the “Time-over-
 122 Threshold” trigger (ToT) and at least 13 bins (i.e. > 325 ns) in 120 FADC

¹For detectors with only two (one) operating PMTs the threshold is 2 (2.8) I_{VEM}^{peak} .

123 bins of a sliding window of $3\mu\text{s}$ are required to be above a threshold of 0.2
 124 I_{VEM}^{peak} in coincidence in 2 out of 3 PMTs². This trigger is intended to select
 125 sequences of small signals spread in time. The ToT trigger is thus optimised
 126 for the detection of near-by, low energy showers, dominated by the electro-
 127 magnetic component, or for high-energy showers where the core is distant.
 128 The time spread arises from a combination of scattering (electromagnetic
 129 component) and geometrical effects (muons) as discussed in [8, 9] where de-
 130 tails are given of how the time spread depends on distance and zenith angle.
 131 Since the average signal duration of a single muon is only about 150 ns, the
 132 time spread of the ToT (325 ns) is very efficient at eliminating the random
 133 muon background. The ToT rate at each detector is $< 2\text{Hz}$ and is mainly
 134 due to the occurrence of two muons arriving within $3\mu\text{s}$, the duration of the
 135 sliding window.

136 The **T2** is applied in the station controller to reduce to about 20 Hz the
 137 rate of events per detector. This reduction is done to cope with the band-
 138 width of the communication system between the detectors and the central
 139 campus. The T2 triggers, namely their time stamp and the kind of T2, are
 140 sent to the CDAS for the formation of the trigger of the array. All ToT-T1
 141 triggers are promoted to the T2 level, whereas TH-T1 triggers are requested
 142 to pass a further higher threshold of $3.2 I_{VEM}^{peak}$ in coincidence among the three
 143 PMTs³. The rates of the TH-T2 triggers are rather uniform in the detectors
 144 over the whole array within a few percent, while those due to the ToT-T2
 145 are less uniform. This is due to the fact that the ToT is very sensitive to the
 146 shape of the signal, this in turn depending on the characteristics of the water,
 147 the reflective liner in the detector and the electronic pulse shaper. However,
 148 the lack of uniformity of the trigger response over the array does not af-
 149 fect the event selection or reconstruction above the energy corresponding to
 150 saturated acceptance.

151 3.2. Trigger of the surface array

152 The third level trigger, **T3**, initiates the central data acquisition from the
 153 array. It is formed at the CDAS, and it is based on the spatial and temporal
 154 combination of T2. Once a T3 is formed, all FADC signals from detectors

²For detectors with only two (one) operating PMTs, the algorithm is applied to two (one) PMTs.

³For detectors with only two (one) operating PMTs the threshold is set to 3.8 (4.5) I_{VEM}^{peak} .

155 passing the T2 are sent to the CDAS, as well as those from detectors passing
156 the T1 but not the T2, provided that they are within $30 \mu\text{s}$ of the T3.

157 The trigger of the array is realised in two modes. The first T3 mode
158 requires the coincidence of at least three detectors that have passed the ToT
159 condition and that meet the requirement of a minimum of compactness,
160 namely, one of the detectors must have one of its closest neighbours and
161 one of its second closest neighbours triggered. It is called " $ToT2C_1\&3C_2$ ",
162 where C_n indicates the n^{th} set of neighbours (see figure 2). Once the spatial
163 coincidence is verified, timing criteria are imposed: each T2 must be within
164 $(6 + 5C_n)\mu\text{s}$ of the first one. An example of such T3 configuration is shown
165 in figure 2, left. Since the ToT as a local trigger has very low background,
166 this trigger selects predominantly physics events. The rate of this T3 with
167 the full array in operation is around 1600 events per day, meaning that each
168 detector participates in an event about 3 times per day. This trigger is
169 extremely pure since 90% of the selected events are real showers and it is
170 mostly efficient for showers below 60° . The 10% remaining are caused by
171 chance coincidences due to the permissive timing criteria. The second T3
172 mode is more permissive. It requires a four-fold coincidence of any T2 with
173 a moderate compactness. Namely, among the four fired detectors, within
174 appropriate time windows, at least one must be in the first set of neighbours
175 from a selected station (C_1), another one must be in the second set (C_2)
176 and the last one can be as far as in the fourth set (C_4). This trigger is
177 called " $2C_1\&3C_2\&4C_4$ ". Concerning timing criteria, we apply the same logic
178 as for the " $ToT2C_1\&3C_2$ ". An example of such T3 configuration, is shown
179 in figure 2, right. Such a trigger is efficient for the detection of horizontal
180 showers that, being rich in muons, generate in the detectors signals that have
181 a narrow time spread, with triggered detectors having wide-spread patterns
182 on the ground. With the full array configuration, this trigger selects about
183 1200 events per day, out of which about 10% are real showers.

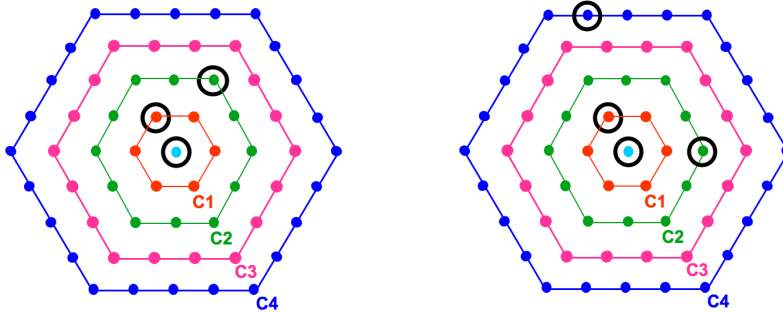


Figure 2: Example of T3 configurations: the 3-fold T3 mode $ToT2C_1\&3C_2$ is shown on the left and the 4-fold mode $2C_1\&3C_2\&4C_4$ on the right (see text for the definitions). C1, C2, C3, C4 indicate the first, second, third and fourth sets of neighbours, respectively at 1.5, 3, 4.5 and 6 km from a given detector.

184 *3.3. Efficiency of the single detector trigger*

185 The single detector trigger probability as a function of the signal, $\mathcal{P}(S)$,
 186 besides being important for the determination of the efficiency of the trigger
 187 of the array, is also of use in the event reconstruction where non-triggered
 188 detectors are included up to 10 km from a triggered one [10].

189 The T1 efficiency versus signal in the detector, $\mathcal{P}(S)$, is determined by
 190 using the very large statistics of EAS ($\approx 10^6$) recorded by the surface detector
 191 array. For each detected EAS, and each participating detector, we measure
 192 the trigger probability $\mathcal{P}(S)$ as the ratio $\frac{N_T(S)}{N_{ON}(S)}$, in different bins of θ and
 193 $S(1000)$, of the number of triggered stations, N_T , to the total number of
 194 active stations, N_{ON} . S is the *expected* signal at a detector, based upon the
 195 LDF fitted from the *measured* values from each detector, and $S(1000)$ is the
 196 signal strength at 1 km, as derived from this fit. Since $\mathcal{P}(S)$ is obtained from
 197 events that actually produced a T3, the method is biased by events with a
 198 positive fluctuation in the signal. This bias can be corrected by Monte Carlo
 199 simulations and is found to be negligible at energies above around 3×10^{18}
 200 eV. Limiting the analysis to showers with $S_{38} > 16$ VEM (corresponding to
 201 about 3×10^{18} eV), the trigger probability versus signal is derived averaging
 202 over all the bins in θ and $S(1000)$. This is shown in figure 3 (circles): the
 203 probability becomes $> 0.95\%$ for $S \approx 10$ VEM. This result is confirmed by an
 204 independent analysis that makes use of showers triggering certain detectors
 205 that have been specially located very close to one another. The surface
 206 array has seven positions in which three detectors (so called triplets) have
 207 been deployed at 11 m from each other. In each triplet, only one detector

208 (master) sends T2 to CDAS, while the other two (slaves) are independently
 209 read out each time a T3 is generated and if they pass the T1. For each
 210 slave, the trigger probability versus recorded signal S is derived from the
 211 ratio between the number of events where both slaves have triggered and
 212 the number of events where only the other one has triggered. Depending if
 213 one or two slaves have triggered, S is either the signal of the only triggered
 214 detector or the average of the two.

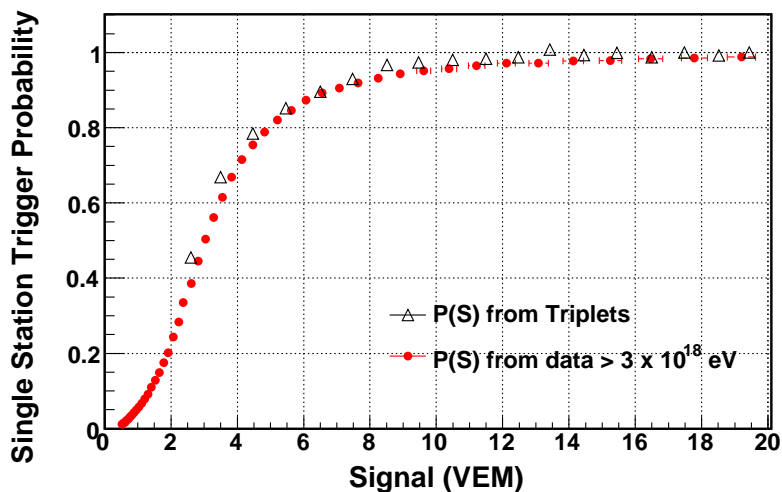


Figure 3: Single detector trigger probability as a function of the signal in the detector, $\mathcal{P}(S)$, obtained from triplets data (triangles) and from showers data with $E > 3 \times 10^{18}$ eV (circles).

215 From the analysis of about 10000 events, and combining the probabilities
 216 for the two slaves, $\mathcal{P}(S)$ is obtained and it is shown in figure 3 (triangles), in
 217 good agreement with the one obtained by showers data.

218 4. Event selection of the surface detector array for showers with 219 zenith angle below 60°

220 A selection of physics events and of detectors belonging to each event is
 221 made after data acquisition. Indeed, a large number of chance coincidence
 222 events is expected due to the large number of possible combinations among
 223 the single detectors. We focus here on the selection of events between 0° and
 224 60° since more inclined showers have different properties and require specific
 225 selection criteria described elsewhere [12].

226 Two successive levels of selection are implemented. The first one (physics
 227 trigger) is based on space and time configurations of the detector, besides
 228 taking into account the kind of trigger in each of them. The second one
 229 (fiducial trigger) requires that the shower selected by the physics trigger is
 230 contained within the array boundaries, to guarantee the accuracy of the event
 231 reconstruction both in terms of arrival direction and energy determination.
 232 The logic of this off-line trigger system and its connection to the DAQ triggers
 233 is summarised in figure 4.

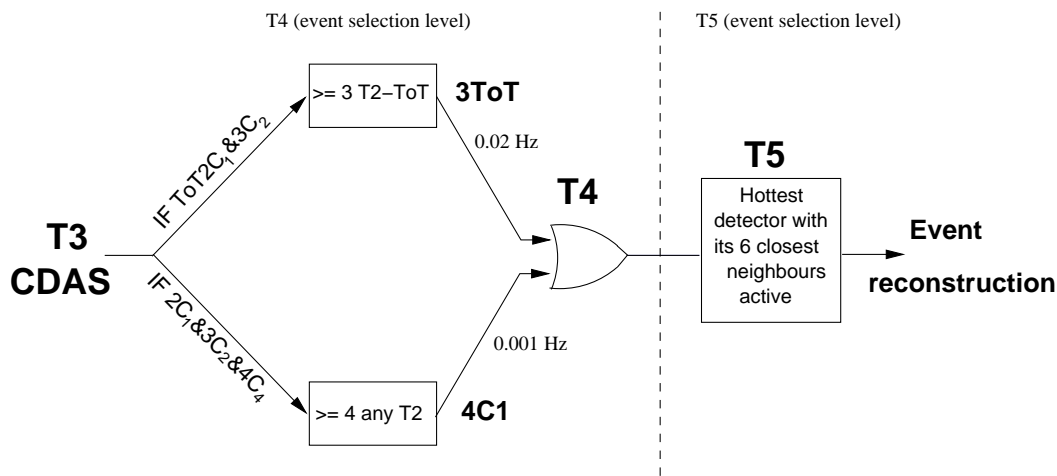


Figure 4: Schematics of the hierarchy of the event selection of the Auger surface detector.

234 4.1. Physics trigger

235 The physics trigger, **T4**, is needed to select real showers from the set of
 236 stored T3 data. Two criteria are defined, with different aims. The first T4
 237 criterion, so-called 3ToT, requires 3 nearby stations, passing the T2-ToT, in
 238 a triangular pattern. It requires additionally that the times of the signals in
 239 the 3 stations fit to a plane shower front moving at the speed of the light.
 240 The number of chance coincidence passing the 3ToT condition over the full
 241 array is less than one per day, thanks to the very low rate of the T2-ToT.
 242 Due to their compactness, events with zenith angles below 60° are selected
 243 with high efficiency, i. e. more than 98%.

244 The second T4 criterion, so called 4C1, requires 4 nearby stations, with
 245 no condition on the kind of T2. In this case also, it is required that the
 246 times of the signals in the 4 stations fit to a plane shower front moving at

247 the speed of the light. This 4C1 trigger brings to $\approx 100\%$ the efficiency for
 248 showers below 60° .

249 The zenith angle distribution of events selected by the T4 criteria is shown
 250 in figure 5, left, in the unfilled histogram for 3ToT, and in the filled one for
 251 the 4C1 that are not 3ToT: the two criteria are clearly complementary, the
 252 latter favouring the selection of events with larger zenith angles. In figure 5,
 253 right, the energy distributions of events selected by the two different criteria
 254 are shown: those selected by 3ToT have a median energy around 6×10^{17}
 255 eV, while for those selected by 4C1 it is around 3×10^{18} eV.

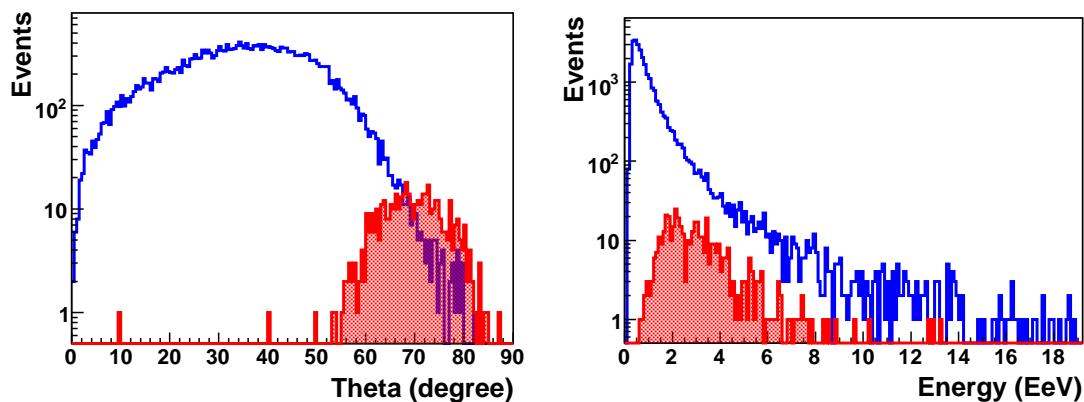


Figure 5: Left: Angular (left) and energy (right) distribution of events selected by the T4 triggers: 3ToT (unfilled histogram), and 4C1, not ToT (filled histogram).

256 Besides disentangling accidental events, there is also the need to identify,
 257 and reject, accidental detectors in real events, i.e. detectors whose signals
 258 are by chance in time with the others, but that in fact are not part of the
 259 event. To this aim, we define a "seed" made by 3 neighbouring detectors in
 260 a non-aligned configuration. If there is more than one triangle of stations,
 261 the seed with the highest total signal is chosen. If the T4 is a 3ToT, only
 262 ToT detectors can be considered to define the seed; if it is a 4C1, also TH
 263 detectors can be included. Once the triangle has been determined, the arrival
 264 direction is estimated by fitting the arrival times of the signals to a plane
 265 shower front moving with the speed of light. Subsequently, all other detectors
 266 are examined, and are defined as accidental if their time delay with respect
 267 to the front plane is outside a time window of $[-2 \mu s : +1 \mu s]$. Detectors that

268 have no triggered neighbours within 3km are always removed.

269 After the selection chain (both event selection and accidental detectors
270 removal), 99.9% of the selected events pass the full reconstruction procedure,
271 that is arrival direction, core position and $S(1000)$ are determined.

272 4.2. Fiducial trigger

273 The need for a *fiducial trigger*, **T5**, mainly arises from events falling close
274 to the border of the array, where a part of the shower may be missing. In
275 figure 6 a hybrid event is shown, that triggered the SD and one of the FD
276 telescopes, where a part of the SD information is missing due to its position
277 on the border of the array.

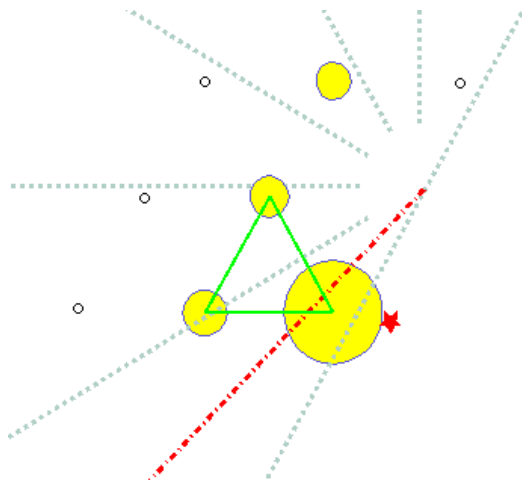


Figure 6: Example of a hybrid, non-T5, event: the event falls on the border of the SD array, triggering only four detectors. Filled circles indicate the triggered ones, open circles the non-triggered active ones. The dimensions of the filled circles are proportional to the measured signal. The shower detector plane reconstructed by FD (dash-dotted line) indicates that the core is within the triangle of detectors. The SD only reconstruction places it outside the array (cross), artificially increasing the event energy.

278 Such events could have wrong core positions, and consequently, incor-
279 rect energies, as in this example where the energy derived by SD is more
280 than 4 times larger than the one estimated by FD (1.4×10^{19} eV instead
281 of 3×10^{18} eV). The main task of the fiducial trigger is thus to select only
282 events well contained in the array, ensuring that the shower core is properly
283 reconstructed.

284 The fiducial trigger should be applied a priori on the events, to be inde-
 285 pendent of the reconstruction procedure. The T5 adopted requires that the
 286 detector with the highest signal has all its 6 closest neighbours working at
 287 the time of the event (i.e., it must be surrounded by a working hexagon).
 288 This ensures adequate containment of the event inside the array. Even in the
 289 case of a high energy event that falls inside, but close to the border of the
 290 array, where part of the data may be missing, information from the seven
 291 detectors closest to the shower core ensures a proper reconstruction. Apply-
 292 ing this condition, the maximum statistical uncertainty in the reconstructed
 293 $S(1000)$ due to event sampling by the array is $\approx 3\%$ [10]. It has to be noted
 294 that this criterion also discards events that, though contained, fall close to
 295 a non-working detector: this is an important issue because, due to the large
 296 number of detectors distributed over 3000 km^2 , about 1% of the detectors are
 297 expected to be not functioning at any moment, even with constant detector
 298 maintenance. For the fully completed array, and taking this into account,
 299 the application of the T5 condition reduces the effective area by 10% with
 300 respect to the nominal one.

301 Finally, the use of the fiducial trigger allows the effective area of the array
 302 to saturate to the geometrical one above a certain primary energy. Indeed,
 303 with no conditions on event containment, the acceptance would increase with
 304 increasing energy, since showers falling outside the borders of the array might
 305 still trigger sufficient detectors to be recorded; the higher their energy, the
 306 farther the distance.

307 **5. Aperture and exposure of the surface detector array for showers** 308 **with zenith angle below 60 degrees**

309 The aperture of the surface detector array is given by the effective area
 310 integrated over solid angle. When the trigger and event selection have full
 311 efficiency, i.e. when the acceptance does not depend on the nature of the
 312 primary particle, its energy or arrival direction, the effective area coincides
 313 with the geometrical one. In subsection 5.1, the energy above which the
 314 acceptance saturates is derived. In section 5.2, the calculation of the exposure
 315 above this energy is detailed.

316 *5.1. Determination of the acceptance saturation energy*

317 **I. From SD data.** The acceptance saturation energy, E_{SAT} , is deter-
 318 mined using two different methods that use events recorded by the surface

319 detector array. In the first one, starting from detected showers, mock events
 320 are generated by fluctuating the amplitude of the signals recorded in each
 321 detector and their arrival time. Such fluctuations are measured [13, 14] by
 322 using twin detectors located at 11 m from each other. To each simulated
 323 event, the full trigger and event selection chain are applied. From the ratio
 324 of the number of triggered events to the simulated, the trigger efficiency is
 325 obtained as a function of energy, as shown in figure 7 (triangles). As can
 326 be seen, the trigger probability becomes almost unity ($> 97\%$) at energy
 327 $E \sim 3 \times 10^{18}$ eV for all angles between 0° and 60° . The fact that the method
 328 is based on the use of showers that actually triggered the array may bias
 329 the estimation of the trigger probability at low energy. However, it does not
 330 bias the result on the trigger probability close to full efficiency, and hence on
 331 E_{SAT} .

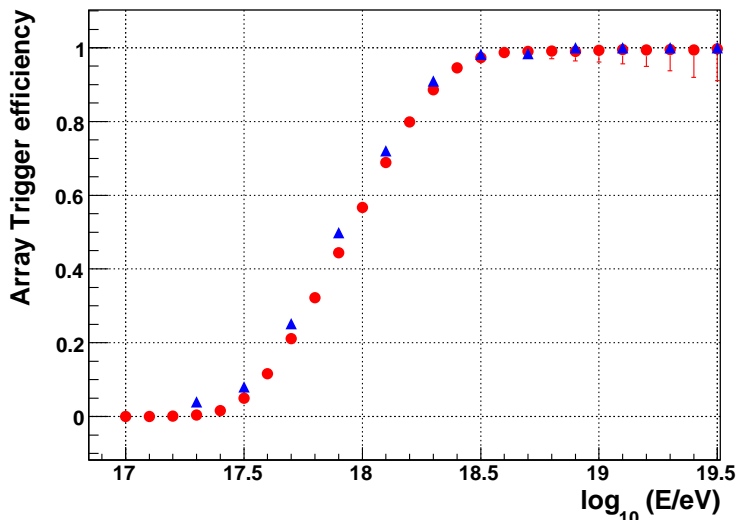


Figure 7: Trigger efficiency as a function of energy, derived from SD data (triangles) and hybrid data (circles).

332 **II. From hybrid data.** The hybrid data sample is composed of events
 333 observed by the FD and that triggered at least one SD detector: consequently,
 334 it has an intrinsically lower energy threshold than the SD. For each bin in
 335 energy (of width 0.2 in $\log_{10}(E)$), the number of events that pass the SD

336 trigger out of the total number of events are counted. To avoid biases from
 337 primary composition, the same data selection criteria as in [15] are used.
 338 Additionally, in analogy with the T5, to avoid the effects of the borders
 339 of the array, it is required that the detector used in the hybrid geometry
 340 reconstruction is surrounded by 6 active detectors. The trigger efficiency of
 341 the surface detector array is found to be saturated ($> 97\%$) for energies
 342 above 3×10^{18} eV, as shown in figure 7 (circles), in agreement with what is
 343 obtained by the analysis of SD data alone.

344 **III. Cross-check with simulations.** E_{SAT} is finally cross-checked using
 345 full shower and detector simulations. The simulation sample consists of
 346 about 5000 proton, 5000 photon and 3000 iron showers simulated using COR-
 347 SIKA [16] with zenith angle distributed as $\sin \theta \cos \theta$ ($\theta < 60^\circ$) and energies
 348 ranging between 10^{17} eV and $10^{19.5}$ eV in steps of 0.25 (0.5 for photons) in
 349 $\log_{10}(E)$. The showers are generated using QGSJET-II [17] and FLUKA [18]
 350 for high and low energy hadronic interactions, respectively. Core positions
 351 are uniformly distributed at ground and each shower is used five times, each
 352 time with a different core position, to increase the statistics with a negligible
 353 degree of correlation. The surface detector array response is simulated using
 354 Geant4 [19] within the framework provided by the Offline software [20]. The
 355 resulting trigger probability as a function of the Monte Carlo energy for pro-
 356 ton, iron and photon primaries is shown in Figure 8 for $0^\circ < \theta < 60^\circ$. Due
 357 to their larger muon content, at low energies iron primaries are slightly more
 358 efficient at triggering the array than protons. However, the trigger becomes
 359 fully efficient at 3×10^{18} eV, both for proton and iron primaries, in different
 360 intervals of zenith angles. It is important to notice that the trigger efficiency
 361 for photons is much lower. This is because photons tend to produce deeper
 362 showers that are poor in muons.

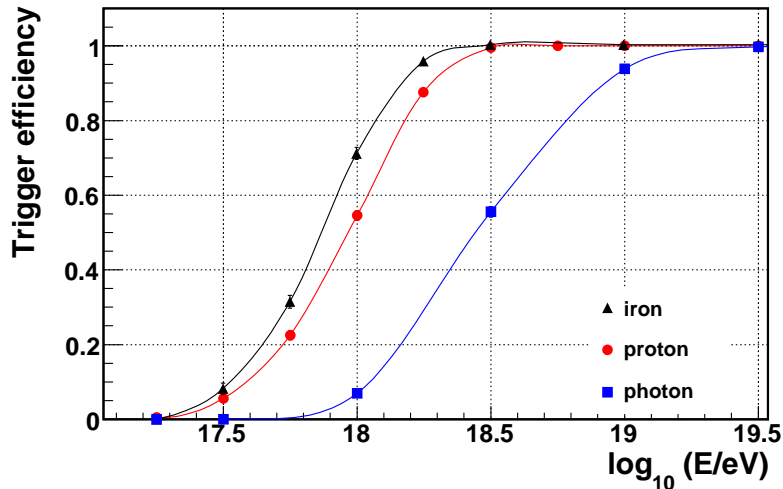


Figure 8: SD trigger efficiency as a function of Monte Carlo energy E for proton (circles), iron (triangles) and photon primaries (squares) and zenith angle integrated up to 60° . Lines are drawn only to guide the eyes.

363 *5.2. Calculation of the integrated exposure*

364 The studies described above have shown that the full efficiency of the
 365 SD trigger and event selection is reached at 3×10^{18} eV. Above this energy,
 366 the calculation of the exposure is based solely on the determination of the
 367 geometrical aperture and of the observation time.

368 With respect to the aperture, the choice of a fiducial trigger based on
 369 hexagons, as explained in section 4.2, allows us to exploit the regularity of
 370 the array very simply. The aperture of the array is obtained as a multiple of
 371 the aperture of an elemental hexagon cell, a_{cell} , defined as any active detector
 372 with six active neighbours, as shown in figure 9.

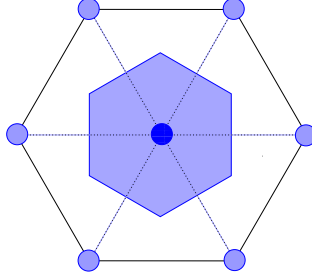


Figure 9: Scheme of an hexagon of detectors: the elemental hexagon cell, a_{cell} , is the shaded area around the central detector.

373 At full efficiency, the detection area per cell is 1.95 km^2 . The correspond-
 374 ing aperture for showers with $\theta < 60^\circ$ is then $a_{\text{cell}} \simeq 4.59 \text{ km}^2 \text{ sr}$. The number
 375 of cells, $N_{\text{cell}}(t)$, is not constant over time due to temporary problems at the
 376 detectors (e. g. failures of electronics, power supply, communication system,
 377 etc...). $N_{\text{cell}}(t)$ is monitored second by second: we show in figure 10 the evo-
 378 lution of $N_{\text{cell}}(t)$ between the start of the data taking, January 2004, and
 379 December 2008. Such precise monitoring of the array configurations allows
 380 us to exploit data during all deployment phases, clearly visible in the figure,
 381 as well as during unstable periods as during, for example, January 2008 when
 382 huge storms affected the communication system.

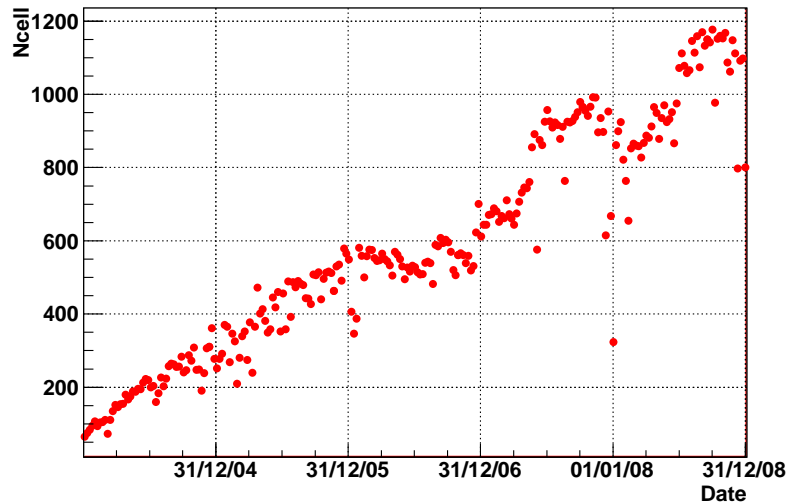


Figure 10: Evolution of the number of hexagonal cells (see text) between January 1st, 2004 and December 31st, 2008

383 The second-by-second monitoring provides at the same time the aperture
 384 of the array per second, $a_{\text{cell}} \times N_{\text{cell}}(t)$, as well as the observation time with
 385 high precision. To calculate the integrated exposure over a given period of
 386 time, the aperture of the array, $N_{\text{cell}}(t) \times a_{\text{cell}}$, is integrated over the number of
 387 live seconds. This calculation is expected to be very precise, since it is based
 388 on a purely geometrical aperture and a very good time precision. However
 389 both the determination of $N_{\text{cell}}(t)$ and of the observation time are affected
 390 by uncertainties.

391 Concerning the determination of $N_{\text{cell}}(t)$, to evaluate the uncertainty in
 392 the number of active detectors, a check of the consistency of the event rate of
 393 each detector with its running time, determined from the monitoring system,
 394 is performed. The uncertainty derived from this study is added to that due
 395 to errors of communication between the station and the DAQ, which are also
 396 monitored. Overall, the uncertainty on the determination of $N_{\text{cell}}(t)$ amounts
 397 to about 1.5%.

398 For the determination of the observation time, and related uncertainty,
 399 the dead time that is unaccounted for in the second by second monitoring

400 of the array, is taken into account⁴. To determine these, an empirical tech-
 401 nique is exploited, based on the study of the distribution of the arrival times
 402 of events, under the reasonable hypothesis that they follow a Poisson dis-
 403 tribution. Given the constant rate λ for the T5 event rate per hexagon,
 404 $\lambda \approx 1.4 \times 10^{-5}$ event per second per hexagon, the probability P that the
 405 time interval T between two consecutive T5 events be larger than T is given
 406 by: $P(T) = e^{-\lambda T}$. We define intervals as dead time if the Poisson probability
 407 of their occurrence is less than 10^{-5} . As an example, we show in figure 11
 408 the distribution of time differences for events acquired in 2008. The distribu-
 409 tion is exponential with a time constant of 72.4 seconds, as expected for the
 410 above value of λ and the observed average number of live hexagons during
 411 that year. In the figure, the points outside the filled area show those time
 412 intervals that have occurred with a Poisson probability less than 10^{-5} .

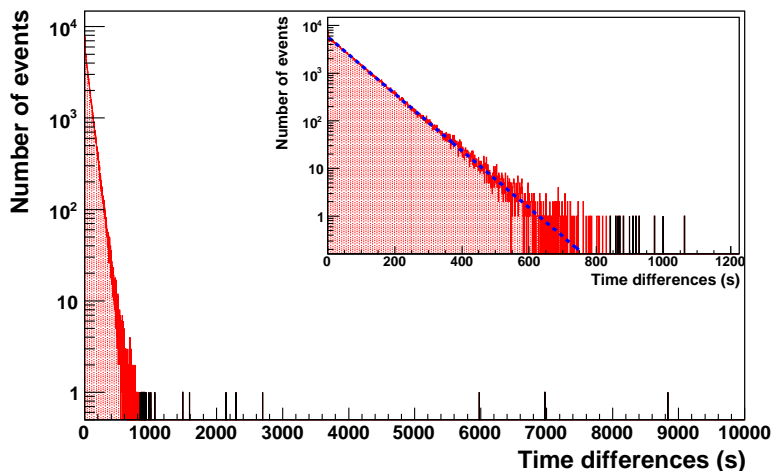


Figure 11: Distribution of time differences between events in 2008. The points outside the filled area show the dead times (see text). The exponential fit is shown as a dashed line in the inset where the histograms are zoomed.

413 The identified dead times generally correspond to periods of software

⁴This dead time can be due either to problems in the communication between the stations and the CDAS or to problems of data storage in the stations

414 modifications at the level either of the single detectors or of the CDAS. These
415 were rather frequent during the deployment phase of the surface detector
416 array, which lasted until June 2008. The uncertainty in the determination
417 of the livetime is estimated to be around 1%. Between January 2004 and
418 December 2008, the livetime of the surface detector array data acquisition is
419 96%. Hidden dead times reduce the effective livetime to 87%, the reduction
420 being mostly due to the two first years of operation. However, due to the
421 growth of the surface detector array, their impact on the total integrated
422 exposure is a reduction of only 3%.

423 6. Conclusions

424 The DAQ trigger of the surface detector array of the Pierre Auger Ob-
425 servatory is organised in a hierarchical way, starting at the level of the single
426 detector (T1, T2) up to the data acquisition (T3). The selection of events
427 below 60° takes place off-line, and it is also hierarchical (T4, T5). The whole
428 chain, from the single detector trigger, up to event selection, is able to re-
429 duce the counting rate of the single detector from about 3 kHz, due mainly
430 to single, uncorrelated, cosmic muons, down to about 3×10^{-5} Hz. This
431 final rate is due to extensive air showers, more than 99% of which pass the
432 reconstruction chain.

433 In spite of the large number of detectors and the possible number of
434 chance events due to combinatorial coincidences among the detectors, the
435 high-purity Time Over Threshold trigger enables the main trigger of the
436 array to be kept at the level of a 3-fold coincidence, thus extending the
437 range of physics that can be studied. Such a trigger, together with the
438 event selection strategy, allows the acquisition and reconstruction of about
439 one cosmic ray shower per minute, with median energy around 6×10^{17} eV.
440 Moreover, it makes the surface detector array fully efficient for showers due to
441 primary cosmic rays above 3×10^{18} eV, independent of their mass and arrival
442 directions. The trigger provides at the same time a larger overlapping energy
443 region with the FD, which is naturally efficient at lower energies, allowing
444 the measurement of the cosmic ray spectrum down to 10^{18} eV [21].

445 Above 3×10^{18} eV, the calculation of the exposure is purely geometrical,
446 being the integration of the geometrical aperture over the observation time.
447 Both of them are known with high precision, so that the overall uncertainty
448 on the integrated exposure is less than 3%. The integrated SD exposure as a
449 function of time is shown in figure 12, from January 2004 to December 2008:

450 at the end of the period it amounts to $12790 \pm 380 \text{ km}^2 \text{ sr yr}$. Even though the
 451 SD was under continuous deployment until June 2008, the effective livetime of
 452 the surface detector array averaged over all the five years is high, being 87%.
 453 The effective livetime of the SD is 96% for 2008 alone: with this livetime and
 454 the full surface detector array deployed, the exposure is expected to increase
 455 by about $500 \text{ km}^2 \text{ sr yr}$ per month.

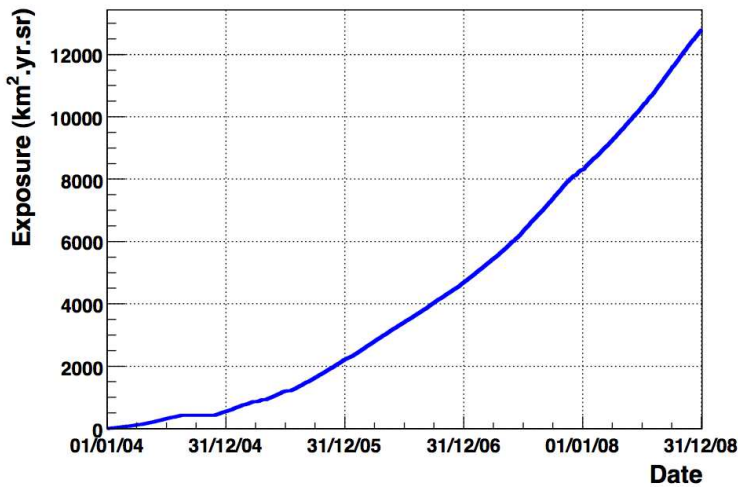


Figure 12: Evolution of the integrated exposure between January 1st, 2004 and December 31st, 2008

456 7. Acknowledgements

457 The successful installation and commissioning of the Pierre Auger Ob-
 458 servatory would not have been possible without the strong commitment and
 459 effort from the technical and administrative staff in Malargüe.

460 We are very grateful to the following agencies and organizations for finan-
 461 cial support: Comisión Nacional de Energía Atómica, Fundación Antorchas,
 462 Gobierno De La Provincia de Mendoza, Municipalidad de Malargüe, NDM
 463 Holdings and Valle Las Leñas, in gratitude for their continuing cooperation
 464 over land access, Argentina; the Australian Research Council; Conselho Na-
 465 cional de Desenvolvimento Científico e Tecnológico (CNPq), Financiadora

466 de Estudos e Projetos (FINEP), Fundação de Amparo à Pesquisa do Es-
467 tado de Rio de Janeiro (FAPERJ), Fundação de Amparo à Pesquisa do Es-
468 tado de São Paulo (FAPESP), Ministério de Ciência e Tecnologia (MCT),
469 Brazil; AVCR AV0Z10100502 and AV0Z10100522, GAAV KJB300100801
470 and KJB100100904, MSMT-CR LA08016, LC527, 1M06002, and MSM00216-
471 20859, Czech Republic; Centre de Calcul IN2P3/CNRS, Centre National
472 de la Recherche Scientifique (CNRS), Conseil Régional Ile-de-France, Dé-
473 partement Physique Nucléaire et Corpusculaire (PNC-IN2P3/CNRS), Dé-
474 partement Sciences de l'Univers (SDU-INSU/CNRS), France; Bundesmin-
475 isterium für Bildung und Forschung (BMBF), Deutsche Forschungsgemein-
476 schaft (DFG), Finanzministerium Baden-Württemberg, Helmholtz-Gemein-
477 schaft Deutscher Forschungszentren (HGF), Ministerium für Wissenschaft
478 und Forschung, Nordrhein-Westfalen, Ministerium für Wissenschaft, For-
479 schung und Kunst, Baden-Württemberg, Germany; Istituto Nazionale di
480 Fisica Nucleare (INFN), Ministero dell'Istruzione, dell'Università e della Ri-
481 cerca (MIUR), Italy; Consejo Nacional de Ciencia y Tecnología (CONA-
482 CYT), Mexico; Ministerie van Onderwijs, Cultuur en Wetenschap, Neder-
483 landse Organisatie voor Wetenschappelijk Onderzoek (NWO), Stichting voor
484 Fundamenteel Onderzoek der Materie (FOM), Netherlands; Ministry of Sci-
485 ence and Higher Education, Grant Nos. 1 P03 D 014 30, N202 090 31/0623,
486 and PAP/218/2006, Poland; Fundação para a Ciência e a Tecnologia, Por-
487 tugal; Ministry for Higher Education, Science, and Technology, Slovenian
488 Research Agency, Slovenia; Comunidad de Madrid, Consejería de Educación
489 de la Comunidad de Castilla La Mancha, FEDER funds, Ministerio de Cien-
490 cia e Innovación, Xunta de Galicia, Spain; Science and Technology Facilities
491 Council, United Kingdom; Department of Energy, Contract No. DE-AC02-
492 07CH11359, National Science Foundation, Grant No. 0450696, The Grainger
493 Foundation USA; ALFA-EC / HELEN, European Union 6th Framework Pro-
494 gram, Grant No. MEIF-CT-2005-025057, European Union 7th Framework
495 Program, Grant No. PIEF-GA-2008-220240, and UNESCO.

496 References

- 497 [1] I. Allekotte et al. (Pierre Auger Collaboration), Nucl. Instr. and Meth.
498 A 586 (2008) 409
- 499 [2] Pierre Auger Collaboration, submitted to Nucl. Instr. and Meth.,
500 arXiv:0907.4282v1 [astro-ph.IM].

- 501 [3] J. Abraham et al. (Pierre Auger Collaboration), Phys. Rev. Lett. 101
502 (2008) 061101
- 503 [4] J. Abraham et al (Pierre Auger Collaboration), Nucl. Instr. and Meth.
504 A 523 (2004) 50
- 505 [5] X. Bertou et al. (Pierre Auger Collaboration), Nucl. Instr. and Meth. A
506 568 (2006) 839
- 507 [6] D. Newton, J. Knapp, A.A. Watson, Astropart. Phys. 26 (2007) 414
- 508 [7] J. Hersil et al., Phys. Rev. Letts. 6 (1961) 22
- 509 [8] J. Linsley and L. Scarsi, Phys. Rev. 128 (1962) 2384
- 510 [9] A.A. Watson and J.G. Wilson, J. Phys. A 7 (1974) 1199
- 511 [10] P.L. Ghia et al. (Pierre Auger Collaboration), Proc. of 29th ICRC,
512 eds. B.S.Acharya et al. Tata Inst. of Fundamental Research, Mumbai, 7
513 (2006) 167
- 514 [11] P. Bauleo et al. (Pierre Auger Collaboration), Proc. of 29th ICRC,
515 eds. B.S.Acharya et al. Tata Inst. of Fundamental Research, Mumbai, 7
516 (2006) 291
- 517 [12] P. Facal San Luis et al. (Pierre Auger Collaboration), Proc. of 30th
518 ICRC, eds. R.Caballero et al., Universidad Nacional Autonoma de Mex-
519 ico, Mexico City, 4 (2008) 339
- 520 [13] M. Ave et al., Nucl. Instr. and Meth. A 578 (2007) 180
- 521 [14] C. Bonifazi et al., Astropart. Phys. 28 (2008) 523
- 522 [15] M. Unger et al. (Pierre Auger Collaboration), Proc. of 30th ICRC, eds.
523 R.Caballero et al., Universidad Nacional Autonoma de Mexico, Mexico
524 City, 4 (2008) 373
- 525 [16] D. Heck, J. Knapp, J.N. Capdevielle, G. Schatz, and T. Thouw, Report
526 FZKA 6019 (1998), Forschungszentrum Karlsruhe
- 527 [17] S. Ostapchenko, Phys.Lett. B 636 (2006) 40, Phys. Rev. D 74 (2006)
528 014026

- 529 [18] G. Battistoni et al., Nucl. Phys. Proc. Suppl. 175 (2008) 88
- 530 [19] S. Agostinelli, J. Allison et al., Nucl. Instr. and Meth. A 506 (2003) 250,
531 IEEE Transactions on Nuclear Science 53 No. 1 (2006) 270
- 532 [20] S. Argirò, S.L.C. Barroso, J. Gonzalez, L. Nellen, T. Paul, T.A. Porter,
533 L. Prado Jr., M. Roth, R. Ulrich, D. Veberič, Nucl. Instr. and Meth. A
534 580 (2007) 1485.
- 535 [21] F. Schüssler et al. (Pierre Auger Collaboration), submitted to Proc. of
536 31st ICRC, Lodz, Poland, 2009